Entanglement Purification and Protection in a Superconducting Quantum Network

Haoxiong Yan,[1,†] Youpeng Zhong,[1†,‡] Hung-Shen Chang,[1] Audrey Bienfait,[1,§] Ming-Han Chou,[1,2] Christopher R. Conner,[1] Étienne Dumur,[1,3,‖] Joel Grebel,[1] Rhys G. Povey,[1,2] and Andrew N. Cleland[1,3,*]

[1]*Pritzker School of Molecular Engineering, University of Chicago, Chicago, Illinois 60637, USA*

[2]*Department of Physics, University of Chicago, Chicago, Illinois 60637, USA*

[3]*Center for Molecular Engineering and Material Science Division, Argonne National Laboratory, Lemont, Illinois 60439, USA*

(Received 22 August 2021; accepted 10 January 2022; published 22 February 2022)

High-fidelity quantum entanglement is a key resource for quantum communication and distributed quantum computing, enabling quantum state teleportation, dense coding, and quantum encryption. Any sources of decoherence in the communication channel, however, degrade entanglement fidelity, thereby increasing the error rates of entangled state protocols. Entanglement purification provides a method to alleviate these nonidealities by distilling impure states into higher-fidelity entangled states. Here we demonstrate the entanglement purification of Bell pairs shared between two remote superconducting quantum nodes connected by a moderately lossy, 1-meter long superconducting communication cable. We use a purification process to correct the dominant amplitude damping errors caused by transmission through the cable, with fractional increases in fidelity as large as 25%, achieved for higher damping errors. The best final fidelity the purification achieves is $94.09 \pm 0.98\%$. In addition, we use both dynamical decoupling and Rabi driving to protect the entangled states from local noise, increasing the effective qubit dephasing time by a factor of 4, from 3 to 12 μs. These methods demonstrate the potential for the generation and preservation of very high-fidelity entanglement in a superconducting quantum communication network.

DOI: 10.1103/PhysRevLett.128.080504

Superconducting qubits are a favored hardware platform for implementing quantum computation, with extant demonstrations of circuits with up to $\sim 10^2$ physical qubits [1–5]. However, there remain significant practical challenges in scaling up to the much larger qubit numbers needed for error correction and for the implementation of useful algorithms [6,7]. Distributed quantum computing provides one path to scaling up, by connecting large numbers of small-scale quantum processors in a quantum network [8–11]. Initial steps have been taken to link small superconducting processors using superconducting transmission lines [12–20], as well as efforts to build coherent microwave-to-optical transducers for optical communication [21,22]. However, other than monolithic demonstrations on a single chip [16], these have not realized the high fidelity entanglement needed for quantum information applications, with photon loss dominating the degradation of coherence during transmission through the cable interconnects, and decay due to local noise limiting the quantum state storage time.

Here we describe a superconducting quantum network with two physically separated nodes, each including three superconducting qubits, connected by a 1-meter superconducting coaxial cable [19]. Using this setup, we can deterministically generate high-fidelity Bell pairs shared between the two nodes by sending microwave photons through the coaxial cable. Amplitude damping of the microwave photons, however, limits the fidelity of the entangled pairs. Here we demonstrate the use of an entanglement purification protocol [23] to correct these errors. Entanglement purification via distillation has been demonstrated in linear optics [24–27], as well as with trapped ions [28] and defects in diamond [29]. In superconducting qubits, mitigating the photon loss in a communication channel has been achieved using adiabatic methods [30] as well as through error-correctable qubits [17]. In contrast to adiabatic protocols which require remote synchronization [30,31], purification protocols can achieve near unit-fidelity Bell states using only local operations. The purification performance should be similar to protocols using error-correctable qubits, but with no additional requirements for intricate qubit encoding and quantum nondemolition measurements [17,32]. Here we show that amplitude damping errors can be effectively corrected by a purification protocol including measurement and postselection. In addition, we use dynamical decoupling (DD) and Rabi driving (RD) [33,34] to protect the entangled states from local decoherence [35,36], effectively increasing the qubit T_2 lifetime by a factor of 4 from 3 to 12 μs. These results provide one possible route for the implementation of high-fidelity distributed quantum computing [8,11,37–39]. Please also see references in the Supplemental Material [40], which includes Refs. [41–44].

An overview of the experiment is shown in Fig. 1, with a schematic in Fig. 1(a), previously described in Ref. [19]. The system comprises two quantum network nodes A and B, where each node includes three capacitively coupled superconducting qubits Q_i^k ($i = 1, 2, 3$; $k = A, B$), based on the xmon design [45,46]. The central qubit Q_2^k in each node is directly coupled to a 1 m-long niobium-titanium (NbTi) superconducting coaxial cable via a tunable coupler G^k [47]. The tunable coupler is connected by superconducting aluminum wire bonds to the center and ground of the coaxial cable [19], effectively forming a Fabry-Pérot cavity with the tunable couplers serving as variable mirrors at either end. When the tunable couplers are turned to near zero coupling strength, the Fabry-Pérot modes have a free spectral range $\omega_{\mathrm{FSR}}/2\pi = 105$ MHz. Here we use the mode at 5.806 GHz mode for communication, with an energy lifetime of $T_{1r} = 477$ ns. The qubits each have a relaxation time of $T_1 \approx 10\ \mu$s and dephasing time $T_2 \approx 3\ \mu$s. Vacuum Rabi oscillations between Q_2^A and the communication mode C are shown in Fig. 1(b), where we excite Q_2^A, then turn on the coupler to coupling strength $g_A/2\pi = 4.3$ MHz while tuning the qubit into resonance with the communication mode; the other coupler is left off, effectively acting as a high-reflectance mirror. The qubit's excited state probability P_e is shown as a function of the interaction time t. More details can be found in Refs. [19,40].

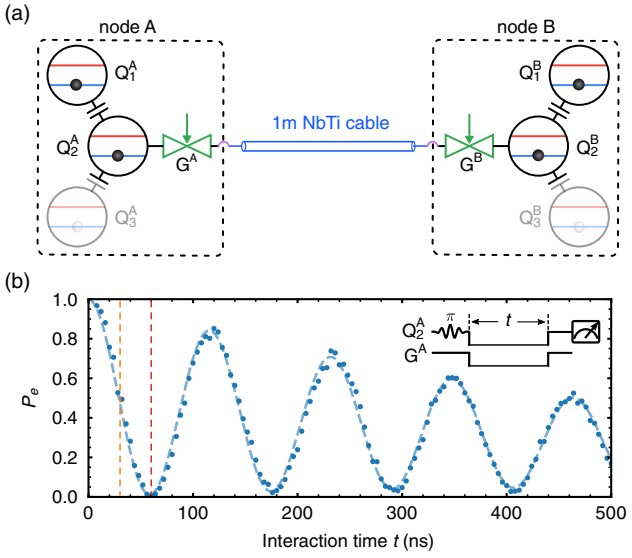

FIG. 1. Device design and vacuum Rabi oscillations. (a) Schematic of the quantum network, comprising two nodes A and B, each with three capacitively coupled xmon qubits $Q_i^{A,B}$ ($i = 1, 2, 3$). The center qubit $Q_2^{A,B}$ in each node is connected to a 1-meter long superconducting NbTi coaxial cable through a tunable coupler $G^{A,B}$. Qubits $Q_3^{A,B}$ are not used in this experiment. (b) Vacuum Rabi oscillations between Q_2^A and the 5.806 GHz communication mode C, measured with coupling strength set to $g^A/2\pi = 4.3$ MHz. Inset shows pulse sequence, where after exciting Q_2^A, the qubit is tuned into resonance with the communication mode while simultaneously turning on the coupler G^A. Blue dashed line is from numerical simulations. The orange and red dashed lines indicate the times for completing a half swap and a full swap of the excitation in Q_2^A to the communication mode.

In Fig. 2 we display the deterministic generation of a Bell state distributed between nodes A and B. Using the tunable coupler, we swap a "half photon" from Q_2^A to Q_2^B with the communication mode C as an intermediate bus. The pulse sequence is shown inset in Fig. 2(a), where we first apply a π pulse to bring Q_2^A from its ground state $|g\rangle$ to its first excited state $|e\rangle$, then turn on Q_2^A's coupler G^A to coupling strength $g^A/2\pi = 4.3$ MHz while tuning Q_2^A into resonance with the communication mode C. The swap time for a full photon emission ($|e0g\rangle \rightarrow i|g1g\rangle$, representing states as $|Q_2^A C Q_2^B\rangle$) is ~60 ns. Here we turn on the coupling for 30 ns, which swaps a half excitation to the cable mode [ideally, $|e0g\rangle \rightarrow (|e0g\rangle + i|g1g\rangle)/\sqrt{2}$]. We then turn off the coupler G^A, and after a time delay t_d, set G^B's coupling strength to $g^B/2\pi = 4.3$ MHz while tuning Q_2^B into resonance with the communication mode. After a 60 ns full swap, this generates a Bell state between Q_2^A and Q_2^B, ideally $|\psi^-\rangle = (|eg\rangle - |ge\rangle)/\sqrt{2}$ (writing the two-qubit state as $|Q_2^A Q_2^B\rangle$). In Fig. 2(a) we show the excited state probability for Q_2^B for two different delay times, $t_d = 50$ ns (orange) and 200 ns (red), along with Q_2^A (blue). These data clearly show the reduction in Q_2^B's excited state probability P_e with delay time t_d.

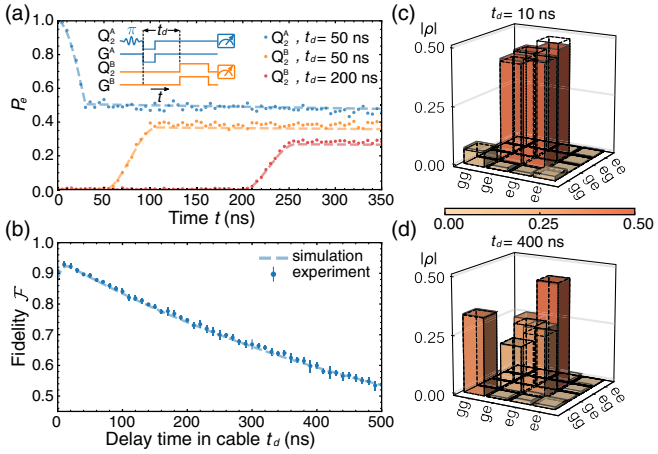

FIG. 2. Deterministic Bell state generation. (a) Inset: Pulse sequence for Bell state generation, including the delay time t_d that the excitation resides in the communication mode C. Main plot shows $|e\rangle$ state population P_e in Q_2^A (blue), and in Q_2^B for different delay times in the cable $t_d = 50$ (orange) and $t_d = 200$ ns (red). (b) Bell state fidelity $\mathcal{F}$ as a function of delay time t_d. (c) Bell state tomography for $t_d = 10$ and (d) $t_d = 400$ ns. Dashed lines in (a) and (b), and dashed outline boxes in (c) and (d), are results from numerical simulations.

In Fig. 2(b) we display the effect of the delay time in the cable t_d on the Bell state fidelity $\mathcal{F}$, defined as $\mathcal{F} = \langle\psi^-|\rho|\psi^-\rangle$, displaying the two-qubit density matrix ρ measured using state tomography [48]. Numerical simulations (dashed blue line; see Supplementary Material Ref. [40]) are in good agreement with the measurements. In Figs. 2(c)–2(d) we show the measured density matrices for the time delays $t_d = 10$ and $t_d = 400$ ns. For the data in Fig. 2(c), the measured fidelity to the ideal Bell state is $\mathcal{F} = 92.89 \pm 0.85\%$, close to the numerical simulation result $\mathcal{F}^{\text{sim}} = 92.01\%$. The data indicate that the dominant infidelity is due to damping errors ($|1\rangle \to |0\rangle$) in the cable, which increase with delay time in the cable, with a much smaller contribution from phase errors in the qubits $(|g\rangle + |e\rangle)/\sqrt{2} \leftrightarrow (|g\rangle - |e\rangle)/\sqrt{2}$. Damping results in a larger $|\text{Tr}(\rho|gg\rangle\langle gg|)|$ component in the density matrix, while phase decoherence yields smaller off-diagonal terms in ρ. From the data at delay $t_d = 400$ ns, we estimate that ~94% of the infidelity is due to damping errors (~82% from cable loss and ~12% from qubit decay) and ~6% is due to qubit decoherence.

We use a purification process including measurement and post-selection to improve the final Bell state fidelities, as shown in Fig. 3. The purification circuit is shown in Fig. 3(a), where two impure Bell pairs $\rho^{(1)}$ and $\rho^{(2)}$ are created between the two nodes, which serve as the source ($\rho^{(1)}$) and target pairs ($\rho^{(2)}$). Parallel CNOT gates are performed between the qubits in each node, followed by Z measurements of the source pair $\rho^{(1)}$, using the measurement results to post-select from $\rho^{(2)}$. The result is a purified Bell pair ρ_f with a higher fidelity to the purification target state $|\psi^+\rangle = (|eg\rangle + |ge\rangle)/\sqrt{2}$ [23].

Including only the errors due to the lossy channel and qubit dephasing, the two nominally identical impure states can be written as

$$\rho^{(1)} = \rho^{(2)} = (1-\epsilon_p)|\psi^-\rangle\langle\psi^-| + \epsilon_p|\psi^+\rangle\langle\psi^+| + \epsilon_d(|gg\rangle\langle gg| - |ge\rangle\langle ge|), \quad (1)$$

where ϵ_d accounts for any damping errors in the cable, of the form $|1\rangle \to |0\rangle$, and ϵ_p accounts for phase errors of the form $(|g\rangle + |e\rangle)/\sqrt{2} \leftrightarrow (|g\rangle - |e\rangle)/\sqrt{2}$, which take $|\psi^-\rangle$ to $|\psi^+\rangle = (|eg\rangle + |ge\rangle)/\sqrt{2}$.

When the two Z measurements of $\rho^{(1)}$ are not consistent, the state ρ_f will be a mixed state, indicating a failed purification. Assuming perfect local operations and measurements, when the two measurement results are consistent, the result is a purified state closer to the ideal $|\psi^+\rangle$ pair. When the measurement result of $\rho^{(1)}$ is $|gg\rangle$, damping errors are partially corrected, with a nonzero ground state $|gg\rangle\langle gg|$ population. For more details see the Supplemental Material [40].

When instead the measurement result is $|ee\rangle$, the final state will be

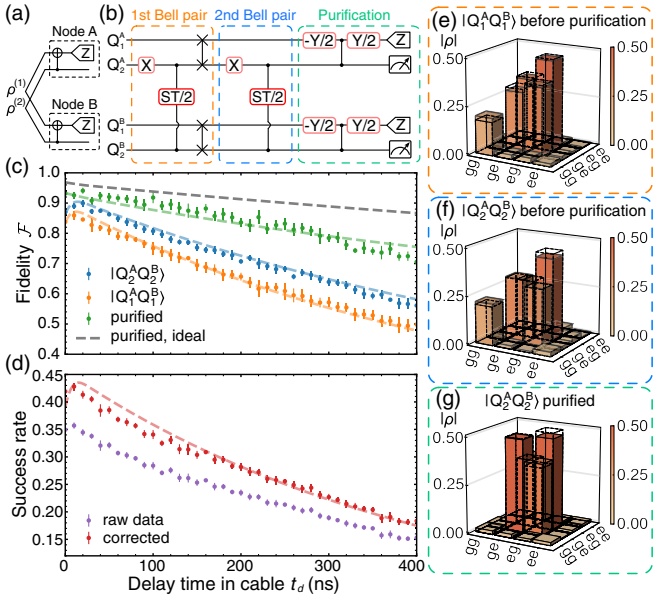

FIG. 3. Entanglement purification. (a) Circuit schematic. (b) Experimental realization of the purification circuit in (a). The ST/2 process is a half-photon transfer process as in Fig. 2(a). We prepare the first Bell pair $|Q_2^AQ_2^B\rangle$ followed by swaps into $|Q_1^AQ_1^B\rangle$. We then generate the second Bell pair in $|Q_2^AQ_2^B\rangle$, and purify using these two pairs. (c) Bell state fidelity $\mathcal{F}$ before purification for $|Q_2^AQ_2^B\rangle$ (blue) and $|Q_1^AQ_1^B\rangle$ (orange), and after purification for $|Q_2^AQ_2^B\rangle$ (green), each measured as a function of delay time t_d. Gray dashed line is for error-free purification between two identical impure Bell states. (d) Success rate for purification, which is the probability of measuring $|Q_1^AQ_1^B\rangle$ in $|ee\rangle$ with (red) and without (purple) readout measurement correction [49]. (e) State tomography with $t_d = 150$ ns for the pre-purification states $|Q_1^AQ_1^B\rangle$, representing $\rho^{(1)}$, with state fidelity $69.4 \pm 2.0\%$, and for (f) $|Q_2^AQ_2^B\rangle$, representing $\rho^{(2)}$, with state fidelity $75.3 \pm 1.0\%$. (g) Tomography for the post-purified $|Q_2^AQ_2^A\rangle$, representing ρ_f, with state fidelity $86.9 \pm 1.8\%$. Dashed lines are simulation results.

$$\rho_f = (1-\epsilon_{p_f})|\psi^+\rangle\langle\psi^+| + \epsilon_{p_f}|\psi^-\rangle\langle\psi^-|, \quad (2)$$

with a phase error $\epsilon_{p_f} = (2\epsilon_p^2 - 2\epsilon_p + 2\epsilon_d)/(1-2\epsilon_d)$ [40]. The damping error is fully corrected, with a purification success rate $0.5 - \epsilon_d$. Here we focus on the measurement result $|ee\rangle$, where the damping error is fully corrected and purification yields higher Bell state fidelities than the $|gg\rangle$ measurement result.

We implement the purification process as shown in Fig. 3(b). After generating the first Bell pair, shared between the two nodes in $|Q_2^AQ_2^B\rangle$, we apply two parallel iSWAP gates that transfer the state to $|Q_1^AQ_1^B\rangle$, with an efficiency over 99%. We then generate the second Bell pair in $|Q_2^AQ_2^B\rangle$ using the same sequence as for the first Bell pair. We indirectly vary the cable loss by changing the delay time t_d the half photon resides in the cable.

Pre-purification measurements of the two Bell states in $|Q_1^A Q_1^B\rangle$ and $|Q_2^A Q_2^B\rangle$, representing $\rho^{(1)}$ and $\rho^{(2)}$, respectively, are shown in Figs. 3(c), 3(e), and 3(f). These indicate the fidelity of the second Bell pair in $|Q_2^A Q_2^B\rangle$ is a few percent lower than the Bell pair in Fig. 2(b), due to imperfections in the iSWAP gates and possible interference with the first Bell pair during the second Bell pair generation. The first Bell pair's fidelity also falls due to qubit decay during the second Bell pair generation. Better qubit lifetimes [50,51], or the use of parallel communication channels, could reduce these infidelities. The purifying CNOT gate, with $|Q_2^A Q_2^B\rangle$ as the control, is implemented using a CZ gate combined with two single-qubit $Y/2$ gates applied to $|Q_1^A Q_1^B\rangle$. The CZ gate is realized using the qubits' second excited state $|f\rangle$, bringing the two-qubit states $|ee\rangle$ and $|gf\rangle$ into energy resonance so that the $|ee\rangle$ state acquires an extra phase compared to the other computational basis states [52]. We typically achieve CZ gate process fidelities of over 95% [40]. Following the CNOT gates, we perform Z measurements of $Q_1^{A,B}$ and tomography measurements of $Q_2^{A,B}$. We postselect as purified states those with $|Q_1^A Q_1^B\rangle = |ee\rangle$; this purification process targets the ideal Bell state $|\psi^+\rangle$.

The fidelity of the purified state, representing ρ_f, is shown in Fig. 3(c) as a function of delay t_d. Larger t_d shows larger purification improvement, as there is more photon loss during cable transmission; the best fidelity of $94.09\% \pm 0.98\%$ is for the shortest delay $t_d = 20$ ns. The largest fractional improvement in fidelity, defined as the change in fidelity divided by the initial (pre-purification) fidelity, is 25%, achieved for the longest delay $t_d = 400$ ns. The success rate, given by the probability of measuring $|Q_1^A Q_1^B\rangle$ in $|ee\rangle$, is shown in Fig. 3(d), which falls for longer delay times, as expected: The main limitation is due to storage decay of the first Bell pair, whose resultingly lower fidelity limits both the success rate and the purified fidelity. The gray dashed line shows the expected purified Bell state fidelity for two identical Bell pairs matching $|Q_2^A Q_2^B\rangle$. State tomography of the purified state for $t_d = 150$ ns is shown in Fig. 4(g), with a state fidelity $86.9 \pm 1.8\%$. The purified state has more than 10% fidelity improvement and damping errors are mostly corrected.

The purification protocol is mostly limited by decoherence in the qubits. The dephasing time $T_2 \sim 3\ \mu$s of our qubits is significantly shorter than the energy relaxation time $T_1 \sim 10\ \mu$s, indicative of extra dephasing channels, possibly due to magnetic flux noise, to which frequency-tunable xmons are particularly susceptible [45]. Using either dynamical decoupling (DD), or a simpler Rabi drive (RD), we can protect the Bell pairs from the local noise that generates some of this decoherence. DD is a technique commonly used in spin systems [33,34], where periodic pulse sequences average the effective environmental noise to near zero, yielding significantly extended

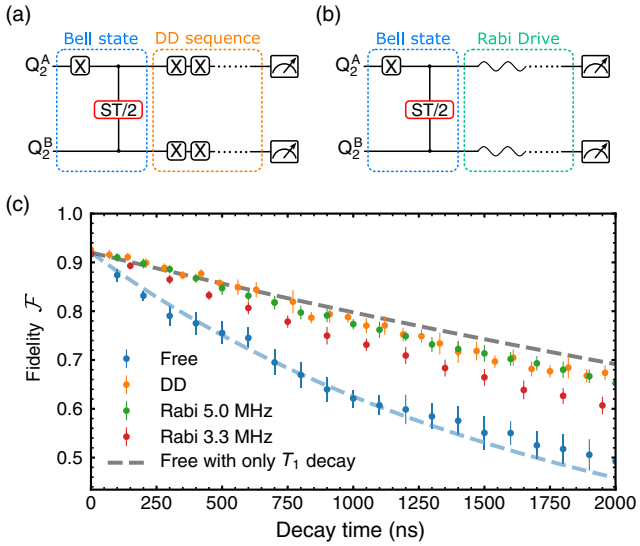

FIG. 4. Entanglement protection using either dynamical decoupling (DD) or Rabi driving. (a) Pulse sequence for DD and (b) Rabi drive. The ST/2 gate corresponds to the half-photon transfer process as shown in Fig. 2(b), with cable delay $t_d = 10$ ns. (c) Bell state fidelity as a function of time for free evolution (blue), DD (orange), and for Rabi drive strengths $\Omega/2\pi = 5$ (green) and $\Omega/2\pi = 3.3$ MHz (red). Numerical simulations are for free evolution including amplitude and phase decay (blue dashed line) and for free evolution with only T_1 decay (gray dashed line).

qubit coherence times [35,36,53], as well as suppression of two-qubit correlated noise [54]. The quantum circuit for DD is shown in Fig. 4(a), where we apply a sequence of X gates to both qubits after generating a Bell state; the simpler RD is shown in Fig. 4(b). The DD X gate we use is a π pulse with an additional DRAG correction [55]. The gate fidelity, as determined by randomized benchmarking [56], is 99.7%, with a gate duration of 30 ns [40]. Following each X gate, we insert 5 ns of buffer time, so that each DD cycle, comprising two X gates, takes 70 ns. To evaluate the performance of the DD sequence, we perform state tomography after a varying number of DD cycles, with the results shown in Fig. 4(d). We see that DD significantly improves the Bell state fidelity, approaching the fidelity associated with pure T_1 dephasing (gray dashed line). For a 1.4 μs evolution time, the state fidelity improves from $57.6 \pm 3.0\%$ to $71.7 \pm 2.3\%$.

The simpler Rabi drive scheme works nearly as well as DD. The fidelity of the Bell pair with Rabi drive is shown in Fig. 4(d), showing similar performance to the DD sequence for $\Omega/2\pi = 5$ MHz. For 1.4 μs evolution, the RD fidelity improves from $57.6 \pm 3.0\%$ to $72.3 \pm 1.5\%$. For both DD and RD, the Bell state fidelity decay corresponds well to simulations using a qubit $T_2 \sim 12\ \mu$s, showing excellent protection of entanglement from local noise. We also tried to combine RD/DD with the purification protocol to further improve the performance. However this was not successful,

we believe because of interference with the frequency-bias pulses applied to $|Q_1^A Q_1^B\rangle$ [40].

In conclusion, we have demonstrated a two-node superconducting quantum network that supports the high-fidelity generation of Bell pairs across the network, with excellent state fidelity of $92.89 \pm 0.85\%$. Purification protocols successfully correct amplitude damping errors caused by the lossy communication channel, improving the state fidelity to $94.09 \pm 0.98\%$. Furthermore, local phase decoherence can be minimized using either dynamical decoupling or the simpler Rabi drive. These results point to the powerful potential for distributed quantum computing in superconducting networks, relying on high-fidelity entanglement over meter-scale networks.

We thank Liang Jiang, David Schuster, and Peter Duda for helpful discussions, and W. D. Oliver and G. Calusine at MIT Lincoln Lab for providing the traveling-wave parametric amplifier (TWPA) used in this work. Devices and experiments were supported by the Air Force Office of Scientific Research and the Army Research Laboratory. É D. was supported by LDRD funds from Argonne National Laboratory; A. N. C. was supported in part by the DOE, Office of Basic Energy Sciences. This work was partially supported by UChicago's MRSEC (NSF Grant DMR-2011854) and by the NSF QLCI for HQAN (NSF Grant 2016136). We made use of the Pritzker Nanofabrication Facility, which receives support from the Soft and Hybrid Nanotechnology Experimental Resource (SHyNE), a node of the National Science Foundation's National Nanotechnology Coordinated Infrastructure (NSF Grant No. NNCI ECCS-2025633).

The authors declare no competing financial interests.

*Corresponding author.
anc@uchicago.edu
†These authors contributed equally to this work.
‡Present address: Shenzhen Institute for Quantum Science and Engineering, Southern University of Science and Technology, Shenzhen 518055, China.
§Present address: Université de Lyon, ENS de Lyon, Université Claude Bernard, CNRS, Laboratoire de Physique, F-69342 Lyon, France.
‖Present address: Université Grenoble Alpes, CEA, INAC-Pheliqs, 38000 Grenoble, France.

[1] R. Barends *et al.*, Superconducting quantum circuits at the surface code threshold for fault tolerance, Nature (London) **508**, 500 (2014).
[2] F. Arute *et al.*, Quantum supremacy using a programmable superconducting processor, Nature (London) **574**, 505 (2019).
[3] P. Jurcevic *et al.*, Demonstration of quantum volume 64 on a superconducting quantum computing system, Quantum Sci. Technol. **6**, 025020 (2021).
[4] M. Gong *et al.*, Quantum walks on a programmable two-dimensional 62-qubit superconducting processor, Science **372**, 948 (2021).
[5] Y. Wu *et al.*, Strong Quantum Computational Advantage using a Superconducting Quantum Processor, Phys. Rev. Lett. **127**, 180501 (2021).
[6] A. G. Fowler, M. Mariantoni, J. M. Martinis, and A. N. Cleland, Surface codes: Towards practical large-scale quantum computation, Phys. Rev. A **86**, 032324 (2012).
[7] J. B. Hertzberg, E. J. Zhang, S. Rosenblatt, E. Magesan, J. A. Smolin, J.-B. Yau, V. P. Adiga, M. Sandberg, M. Brink, J. M. Chow, and J. S. Orcutt, Laser-annealing Josephson junctions for yielding scaled-up superconducting quantum processors, npj Quantum Inf. **7**, 129 (2021).
[8] D. Gottesman and I. L. Chuang, Demonstrating the viability of universal quantum computation using teleportation and single-qubit operations, Nature (London) **402**, 390 (1999).
[9] L. Jiang, J. M. Taylor, A. S. Sørensen, and M. D. Lukin, Distributed quantum computation based on small quantum registers, Phys. Rev. A **76**, 062323 (2007).
[10] H. J. Kimble, The quantum internet, Nature (London) **453**, 1023 (2008).
[11] C. Monroe, R. Raussendorf, A. Ruthven, K. R. Brown, P. Maunz, L.-M. Duan, and J. Kim, Large-scale modular quantum-computer architecture with atomic memory and photonic interconnects, Phys. Rev. A **89**, 022317 (2014).
[12] P. Kurpiers, P. Magnard, T. Walter, B. Royer, M. Pechal, J. Heinsoo, Y. Salathé, A. Akin, S. Storz, J.-C. Besse, S. Gasparinetti, A. Blais, and A. Wallraff, Deterministic quantum state transfer and remote entanglement using microwave photons, Nature (London) **558**, 264 (2018).
[13] C. J. Axline, L. D. Burkhart, W. Pfaff, M. Zhang, K. Chou, P. Campagne-Ibarcq, P. Reinhold, L. Frunzio, S. M. Girvin, L. Jiang, M. H. Devoret, and R. J. Schoelkopf, On-demand quantum state transfer and entanglement between remote microwave cavity memories, Nat. Phys. **14**, 705 (2018).
[14] P. Campagne-Ibarcq, E. Zalys-Geller, A. Narla, S. Shankar, P. Reinhold, L. Burkhart, C. Axline, W. Pfaff, L. Frunzio, R. J. Schoelkopf, and M. H. Devoret, Deterministic Remote Entanglement of Superconducting Circuits through Microwave Two-Photon Transitions, Phys. Rev. Lett. **120**, 200501 (2018).
[15] N. Leung, Y. Lu, S. Chakram, R. K. Naik, N. Earnest, R. Ma, K. Jacobs, A. N. Cleland, and D. I. Schuster, Deterministic bidirectional communication and remote entanglement generation between superconducting qubits, npj Quantum Inf. **5**, 18 (2019).
[16] Y. P. Zhong, H.-S. Chang, K. J. Satzinger, M.-H. Chou, A. Bienfait, C. R. Conner, É. Dumur, J. Grebel, G. A. Peairs, R. G. Povey, D. I. Schuster, and A. N. Cleland, Violating Bell's inequality with remotely connected superconducting qubits, Nat. Phys. **15**, 741 (2019).
[17] L. D. Burkhart, J. D. Teoh, Y. Zhang, C. J. Axline, L. Frunzio, M. Devoret, L. Jiang, S. Girvin, and R. Schoelkopf, Error-detected state transfer and entanglement in a superconducting quantum network, PRX Quantum **2**, 030321 (2021).
[18] P. Magnard, S. Storz, P. Kurpiers, J. Schär, F. Marxer, J. Lütolf, T. Walter, J.-C. Besse, M. Gabureac, K. Reuer, A. Akin, B. Royer, A. Blais, and A. Wallraff, Microwave

Quantum Link between Superconducting Circuits Housed in Spatially Separated Cryogenic Systems, Phys. Rev. Lett. **125**, 260502 (2020).

[19] Y. Zhong, H.-S. Chang, A. Bienfait, É. Dumur, M.-H. Chou, C. R. Conner, J. Grebel, R. G. Povey, H. Yan, D. I. Schuster, and A. N. Cleland, Deterministic multi-qubit entanglement in a quantum network, Nature (London) **590**, 571 (2021).

[20] A. Gold, J. P. Paquette, A. Stockklauser, M. J. Reagor, M. S. Alam, A. Bestwick, N. Didier, A. Nersisyan, F. Oruc, A. Razavi, B. Scharmann, E. A. Sete, B. Sur, D. Venturelli, C. J. Winkleblack, F. Wudarski, M. Harburn, and C. Rigetti, Entanglement across separate silicon dies in a modular superconducting qubit device, npj Quantum Inf. **7**, 142 (2021).

[21] X. Han, W. Fu, C. Zhong, C.-L. Zou, Y. Xu, A. A. Sayem, M. Xu, S. Wang, R. Cheng, L. Jiang, and H. X. Tang, Cavity piezo-mechanics for superconducting-nanophotonic quantum interface, Nat. Commun. **11**, 3237 (2020).

[22] M. Mirhosseini, A. Sipahigil, M. Kalaee, and O. Painter, Superconducting qubit to optical photon transduction, Nature (London) **588**, 599 (2020).

[23] C. H. Bennett, G. Brassard, S. Popescu, B. Schumacher, J. A. Smolin, and W. K. Wootters, Purification of Noisy Entanglement and Faithful Teleportation via Noisy Channels, Phys. Rev. Lett. **76**, 722 (1996).

[24] J.-W. Pan, C. Simon, Č. Brukner, and A. Zeilinger, Entanglement purification for quantum communication, Nature (London) **410**, 1067 (2001).

[25] J.-W. Pan, S. Gasparoni, R. Ursin, G. Weihs, and A. Zeilinger, Experimental entanglement purification of arbitrary unknown states, Nature (London) **423**, 417 (2003).

[26] X.-M. Hu, C.-X. Huang, Y.-B. Sheng, L. Zhou, B.-H. Liu, Y. Guo, C. Zhang, W.-B. Xing, Y.-F. Huang, C.-F. Li, and G.-C. Guo, Long-Distance Entanglement Purification for Quantum Communication, Phys. Rev. Lett. **126**, 010503 (2021).

[27] S. Ecker, P. Sohr, L. Bulla, M. Huber, M. Bohmann, and R. Ursin, Experimental Single-Copy Entanglement Distillation, Phys. Rev. Lett. **127**, 040506 (2021).

[28] R. Reichle, D. Leibfried, E. Knill, J. Britton, R. B. Blakestad, J. D. Jost, C. Langer, R. Ozeri, S. Seidelin, and D. J. Wineland, Experimental purification of two-atom entanglement, Nature (London) **443**, 838 (2006).

[29] N. Kalb, A. A. Reiserer, P. C. Humphreys, J. J. W. Bakermans, S. J. Kamerling, N. H. Nickerson, S. C. Benjamin, D. J. Twitchen, M. Markham, and R. Hanson, Entanglement distillation between solid-state quantum network nodes, Science **356**, 928 (2017).

[30] H.-S. Chang, Y. P. Zhong, A. Bienfait, M.-H. Chou, C. R. Conner, É. Dumur, J. Grebel, G. A. Peairs, R. G. Povey, K. J. Satzinger, and A. N. Cleland, Remote Entanglement via Adiabatic Passage using a Tunably Dissipative Quantum Communication System, Phys. Rev. Lett. **124**, 240502 (2020).

[31] N. V. Vitanov, A. A. Rangelov, B. W. Shore, and K. Bergmann, Stimulated Raman adiabatic passage in physics, chemistry, and beyond, Rev. Mod. Phys. **89**, 015006 (2017).

[32] W. Dür and H. J. Briegel, Entanglement purification and quantum error correction, Rep. Prog. Phys. **70**, 1381 (2007).

[33] H. Y. Carr and E. M. Purcell, Effects of diffusion on free precession in nuclear magnetic resonance experiments, Phys. Rev. **94**, 630 (1954).

[34] S. Meiboom and D. Gill, Modified spin-echo method for measuring nuclear relaxation times, Rev. Sci. Instrum. **29**, 688 (1958).

[35] J. Bylander, S. Gustavsson, F. Yan, F. Yoshihara, K. Harrabi, G. Fitch, D. G. Cory, Y. Nakamura, J.-S. Tsai, and W. D. Oliver, Noise spectroscopy through dynamical decoupling with a superconducting flux qubit, Nat. Phys. **7**, 565 (2011).

[36] B. Pokharel, N. Anand, B. Fortman, and D. A. Lidar, Demonstration of Fidelity Improvement using Dynamical Decoupling with Superconducting Qubits, Phys. Rev. Lett. **121**, 220502 (2018).

[37] J. F. Fitzsimons, Private quantum computation: An introduction to blind quantum computing and related protocols, npj Quantum Inf. **3**, 23 (2017).

[38] K. S. Chou, J. Z. Blumoff, C. S. Wang, P. C. Reinhold, C. J. Axline, Y. Y. Gao, L. Frunzio, M. H. Devoret, L. Jiang, and R. J. Schoelkopf, Deterministic teleportation of a quantum gate between two logical qubits, Nature (London) **561**, 368 (2018).

[39] Y. Wan, D. Kienzler, S. D. Erickson, K. H. Mayer, T. R. Tan, J. J. Wu, H. M. Vasconcelos, S. Glancy, E. Knill, D. J. Wineland, A. C. Wilson, and D. Leibfried, Quantum gate teleportation between separated qubits in a trapped-ion processor, Science **364**, 875 (2019).

[40] See Supplemental Material at http://link.aps.org/supplemental/10.1103/PhysRevLett.128.080504 for more details regarding device characterization and numerical simulations.

[41] E. Jeffrey, D. Sank, J. Y. Mutus, T. C. White, J. Kelly, R. Barends, Y. Chen, Z. Chen, B. Chiaro, A. Dunsworth, A. Megrant, P. J. J. O'Malley, C. Neill, P. Roushan, A. Vainsencher, J. Wenner, A. N. Cleland, and J. M. Martinis, Fast Accurate State Measurement with Superconducting Qubits, Phys. Rev. Lett. **112**, 190504 (2014).

[42] C. Macklin, K. O'Brien, D. Hover, M. E. Schwartz, V. Bolkhovsky, X. Zhang, W. D. Oliver, and I. Siddiqi, A near-quantum-limited Josephson traveling-wave parametric amplifier, Science **350**, 307 (2015).

[43] K. Fujii and K. Yamamoto, Entanglement purification with double selection, Phys. Rev. A **80**, 042308 (2009).

[44] S. Krastanov, V. V. Albert, and L. Jiang, Optimized entanglement purification, Quantum **3**, 123 (2019).

[45] J. Koch, T. M. Yu, J. Gambetta, A. A. Houck, D. I. Schuster, J. Majer, A. Blais, M. H. Devoret, S. M. Girvin, and R. J. Schoelkopf, Charge-insensitive qubit design derived from the Cooper pair box, Phys. Rev. A **76**, 042319 (2007).

[46] R. Barends, J. Kelly, A. Megrant, D. Sank, E. Jeffrey, Y. Chen, Y. Yin, B. Chiaro, J. Mutus, C. Neill, P. O'Malley, P. Roushan, J. Wenner, T. C. White, A. N. Cleland, and J. M. Martinis, Coherent Josephson Qubit Suitable for Scalable Quantum Integrated Circuits, Phys. Rev. Lett. **111**, 080502 (2013).

[47] Y. Chen *et al.*, Qubit Architecture with High Coherence and Fast Tunable Coupling, Phys. Rev. Lett. **113**, 220502 (2014).

[48] M. Steffen, M. Ansmann, R. C. Bialczak, N. Katz, E. Lucero, R. McDermott, M. Neeley, E. M. Weig,

A. N. Cleland, and J. M. Martinis, Measurement of the entanglement of two superconducting qubits via state tomography, Science **313**, 1423 (2006).

[49] R. C. Bialczak, M. Ansmann, M. Hofheinz, E. Lucero, M. Neeley, A. D. O'Connell, D. Sank, H. Wang, J. Wenner, M. Steffen, A. N. Cleland, and J. M. Martinis, Quantum process tomography of a universal entangling gate implemented with Josephson phase qubits, Nat. Phys. **6**, 409 (2010).

[50] M. Reagor, W. Pfaff, C. Axline, R. W. Heeres, N. Ofek, K. Sliwa, E. Holland, C. Wang, J. Blumoff, K. Chou, M. J. Hatridge, L. Frunzio, M. H. Devoret, L. Jiang, and R. J. Schoelkopf, Quantum memory with millisecond coherence in circuit QED, Phys. Rev. B **94**, 014506 (2016).

[51] A. P. M. Place *et al.*, New material platform for superconducting transmon qubits with coherence times exceeding 0.3 milliseconds, Nat. Commun. **12**, 1779 (2021).

[52] T. Yamamoto, M. Neeley, E. Lucero, R. C. Bialczak, J. Kelly, M. Lenander, M. Mariantoni, A. D. O'Connell, D. Sank, H. Wang, M. Weides, J. Wenner, Y. Yin, A. N. Cleland, and J. M. Martinis, Quantum process tomography of two-qubit controlled-Z and controlled-NOT gates using superconducting phase qubits, Phys. Rev. B **82**, 184515 (2010).

[53] J. Qiu *et al.*, Suppressing Coherent Two-Qubit Errors via Dynamical Decoupling, Phys. Rev. Applied **16**, 054047 (2021).

[54] Z. Chen *et al.*, Exponential suppression of bit or phase errors with cyclic error correction, Nature (London) **595**, 383 (2021).

[55] F. Motzoi, J. M. Gambetta, P. Rebentrost, and F. K. Wilhelm, Simple Pulses for Elimination of Leakage in Weakly Nonlinear Qubits, Phys. Rev. Lett. **103**, 110501 (2009).

[56] E. Knill, D. Leibfried, R. Reichle, J. Britton, R. B. Blakestad, J. D. Jost, C. Langer, R. Ozeri, S. Seidelin, and D. J. Wineland, Randomized benchmarking of quantum gates, Phys. Rev. A **77**, 012307 (2008).